Welding in the World (2023) 67:683–705
https://doi.org/10.1007/s40194-022-01432-z

RESEARCH PAPER

Sequence effects on the life estimation of thin-walled welded tubular structures made of HSS + UHSS under bending

Josef Neuhäusler[1] · Jakob Roth[1] · Markus Oswald[1] · André Dürr[1] · Klemens Rother[1]

Received: 15 September 2022 / Accepted: 28 November 2022 / Published online: 12 December 2022

Abstract
Welded hollow sections are typical in different industries. A database of fatigue life data of welded hollow section joints covering sequence effects and the accuracy of the linear damage accumulation is presented. The effects of the shape of the applied load spectra, sequence effects of different amplitudes have been investigated using two high-strength steels. This document covers thin-walled tubes of 2-mm thickness made of low-carbon or mild steel 1.8849 (S460MH) and austenitic TWIP-steel 1.4678 + CP700 (X30MnCrN16-14). Constant amplitude and two-level load spectra are presented to check the linear damage accumulation. Using stress concentration factors from finite element analysis, typical FAT classes for the structural and the effective notch stress concepts are checked as well. Both structures show much higher strength compared IIW recommendations by structural stress approach and DVS 0905 by effective notch stress approach. Typical maximum linear damage sums taken from recommendations and codes of 0.2 or 0.5 are exceeded for all spectra investigated and in some of the cases even significantly above 1.0. Transferability of the recommendations to component type structures like those tubular joints made of high-strength steel needs revision to lift its lightweight potential but this will require additional data.

Keywords Tubular constructions · Carbon steels · Austenitic steels · Fatigue tests · Fatigue strength · Finite element analysis · Variable loading

Nomenclature

Symbol, Abbreviations

A, A_{80} [%]	Elongation after fracture
E [MPa]	Modulus of elasticity
F [N]	Force
c_N [MPa/kN]	Transfer coefficient load vs. nominal stress
D [−]	Damage sum
ΔF [N]	Range of applied forces
ΔS [MPa]	Nominal stress range
D_V [−]	Relative damage D_{test}/D_{calc}
$f(R)$ [−]	Factor for mean stress correction
K_t [−]	Stress concentration factor, SCF
K_w [−]	Seam shape factor σ_k/σ_{hs}
LF [−]	Load factor = magnitude of ratio high vs. low load level
m [−]	Slope exponent of Basquin equation
n [−]	Number of specimens or applied number of cycles
$N_{äq}$ [−]	Equivalent cycle to failure assuming CAL at max. load level of VAL spectrum
P_A [%]	Failure probability
R [−]	Stress ratio min/max stress of cycle
s [−]	Standard deviation
σ [MPa]	Local stress (structural or notch stress)
SR [−]	Stress ratio of characteristic values test vs. IIW/DVS
T [−]	Scatter factor
W [mm^3]	Section modulus

Indices, superscripts

N	Cycle to failure
0.3 mm	Fictitious radius $r = 0.3$ mm at toe and root
1E4	10,000 Cycles
1 mm	Position 1-mm distance from hot spot
2E6	2·106 Cycles
2 mm	Postion 2-mm distance from hot spot
calc	Related to computational analysis
corr	Correction (for small sample)
DVS	DVS 0905

✉ Klemens Rother
klemens.rother@hm.edu

[1] Institute of Material- and Building Research, Munich University of Applied Sciences, Munich, Germany

ES	Residual stress
h	High stress level
hs	Structural or hot-spot stress
IIW	IIW recommendations
ISO	ISO 14347
k	Notch stress
l	Left or low stress level
lgN	Log_{10} of cycle number
lin	Linear extrapolation scheme for structural stress concept
quad	Quadratic extrapolation scheme for structural stress concept
r	Right
spec	Specified cycles for spetra yielding $D=1$ theoretically
test	Related to test results
x%	X-% Probability of failure (2.3%, 10%, 50%, 90%, 97.7%)

Abbreviation

AHSS	Advanced high-strength steel
CAL	Constand amplitude loading
FAT	Characteristic fatigue strength for low $P_A = 2.3\%$, $2 \cdot 10^6$ cycles, and $R = 0.5$
FZ	Fused zone
HAZ	Heat-affected zone
HCF	High cycle fatigue
LCF	Low cycle fatigue
SCF	Stress concentration factor
TWIP	Twinning-induced plasticity
UHSS	Ultra high-strength steel
VAL	Variable amplitude loading

1 Introduction

Hollow sections for lightweight structures are common use in many industrial sectors like crane industry, agricultural and transportation industry, and steel bridge constructions. In general, these tubular structures represent truss or frame like topologies. To lift lightweight potentials in modern designs, use of high- and ultra-high-strength steel grades for an economical design becomes increasingly relevant. Many codes or recommendations are lacking data for designing with high-strength steel. The enormous efforts made by the steel industry in recent years to continuously increase strength and ductility in the form of pareto-optimal new grades (advanced high-strength steels AHSS, ultrahigh-strength steels UHSS) and to make this material available to the industry are not yet visible in the codes and recommendation.

Typically, such tubular structures have to be designed for variable amplitude loading to avoid fatigue damage by the use of linear damage accumulation. Limits of the allowable linear damage sums below 1.0 are used in many of those design rules to compensate somewhat the systematic inaccuracy of the linear damage accumulation. When determining the damage sums, the effects of important influencing factors are not taken into account. Among those are the shape of the amplitude spectrum applied, the influence of rare overloads like misuse, welding residual stresses and their relaxation by service loads, and possible sequence effects by varying load levels in time.

It is well known that an analytical damage sum as obtained by using the linear accumulation by Palmgren [1] and Miner [2] in relation to experimental results of life can scatter very widely and that the specified or recommended allowable limits which might lead to uneconomical or even unsafe designs. Many researchers addressed the topic of the prediction capabilities of the linear damage rule [3–6]. One very large study was done in the 1990's by a German group [7]. Generations of researches are trying to improve the damage accumulation theories for better predictability [8–15]. A comprehensive overview by Fatemi and Yang from 1998 is still a good summary for modifications of the linear damage accumulation theory covering the last century [16].

Among the objectives of this research project as presented in this paper was to verify the application of linear damage accumulation by providing a broad test base of different load sequences for different welded hollow sections made of different steel grades and having different sections to cover the size effect. Here, only thin-walled tubular joints under bending are covered. In a second publication, an investigation of thick-walled welded tubular structures can be found [17].

By using welded hollow sections for testing constant amplitude SN curves as well as experimental fatigue life for a variety of test scenarios, this project provides new data on tested components. It will be shown that the transferability of recommendations from technical rules to components is still an open issue. Rules, standards, and recommendations are usually referring to small specimens for specific welded joints. Size effects due to the size of the weld throats and also size effects due to the length of highly stressed weld toes and roots are not covered sufficiently. This will be demonstrated by the experimental findings in the following.

2 Thin-walled X-hollow section joint under bending

2.1 Materials, specimens, and test setup

For the tests on thin-walled hollow section X joints like bus structures, test specimens are made of two different materials:

Table 1 Monotonic material parameters of 1.4678 + CP700, supplier data taken from coil used to manufacture tubes

Reference		$R_{p0.2}$	R_m	Fracture elongation
prEN 10088–2:2021	Sheet	700–900[2]	750–1000[1]	$A_{80} > 40\%$[1]
Steel supplier	Sheet	819	1041	$A_{80} = 33.6\%$
Tube supplier	Tube	883	1010	$A_5 = 29\%$
EN 10219–1:2006	Tube	460	530–720	$A = 17\%$

[1]Cold rolled strip before work hardening (process route 2H)

[2]CP700 cold worked condition

Table 2 Chemical composition (ranges) as given by supplier in accordance to [19]

Melt		Cr	C	Mn	N
	Min	13.0	0.2	14.0	0.2
	Max	16.0	0.4	18.0	0.4

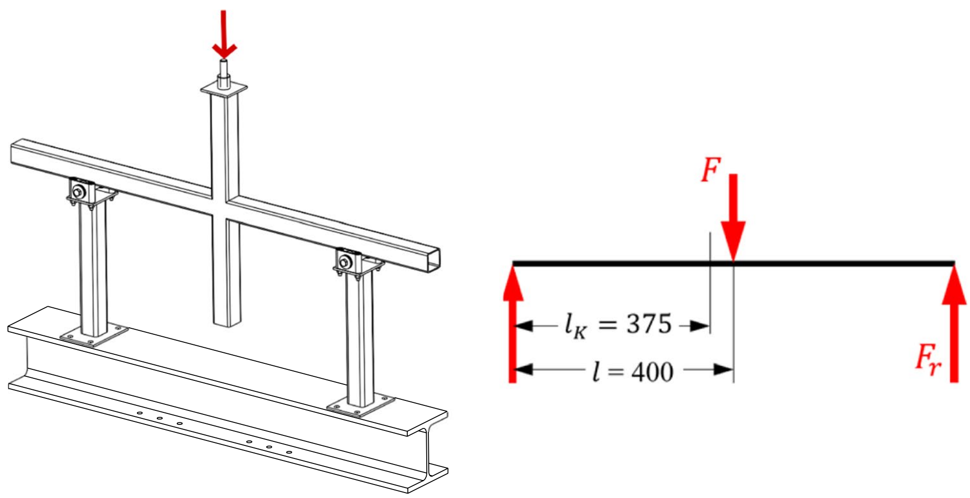

Fig. 1 Setup of the three-point bending test and location of nominal cross section

- The hot-rolled, high-strength, low-alloy steel S460MH (1.8849, EN 10219–1 [18]) having a yield strength of $R_{eH,min} = 420$ MPa, an ultimate tensile strength of $R_m = 500$–660 MPa rupture elongation $A = 19\%$. This mild steel was the selection of a project partner involved from the truck and bus industry and gives a good chance for lowering weight of bus bodies compared to conventional mild steel grades.
- The fully austenitic, ultra-high-strength, and very ductile nickel-free TWIP steel X30MnCrN16-14 (1.4678, prEN **10088-2** [19]). For manufacturing the tubes and after solution annealing, the material was temper-rolled to lift the minimum yield strength up to 800 MPa (1.4678 + CP700). The work-hardened sheet in this condition is supplied by Outokumpu under the trade name Forta 800 having a yield strength of $R_{p0.2} = 800$ MPa, an ultimate tensile strength of $R_m = 1000$ MPa rupture elongation $A_{80} = 31\%$ [20]. The material strength can be lifted up to 1.6 GPa for monotonic loading and for high strain rates up to 2.0 GPa due to intense formation of twins in different planes [21]. This makes this material especially important in case of high-strength requirements for static or crash loading, lightweight design in transportation industry or moving structures for capital goods. See Tables 1 and 2 for monotonic material data for steel sheet and tubes used in the project as well as the range of chemical composition as given by the steel supplier for this type of steel.

In the following text, the low-carbon or mild steel will be referred to as 1.8849 and the austenitic TWIP steel will be referred to as 1.4678.

All tests are carried out on a three-point bending test, the schematic diagram of which can be seen in Fig. 1. The distance between the simple supports is 800 mm.

The dimensions for this type of specimen and test remain constant for all tests performed. The nominal dimensions of the square tubes are all 50 × 50 × 2 mm.

Welding was performed manually for 1.8849 and automatically for 1.4678. For 1.4678, SN curves also have been obtained for a small number of manually welded specimens. No weld preparation has been performed prior to welding. The manual and automated welding processes were performed according to specifications of the industrial partner from bus industry involved. The comparison of manual and automated welding was in the interest of industrial partners. Tack welding of filler rods to the belt

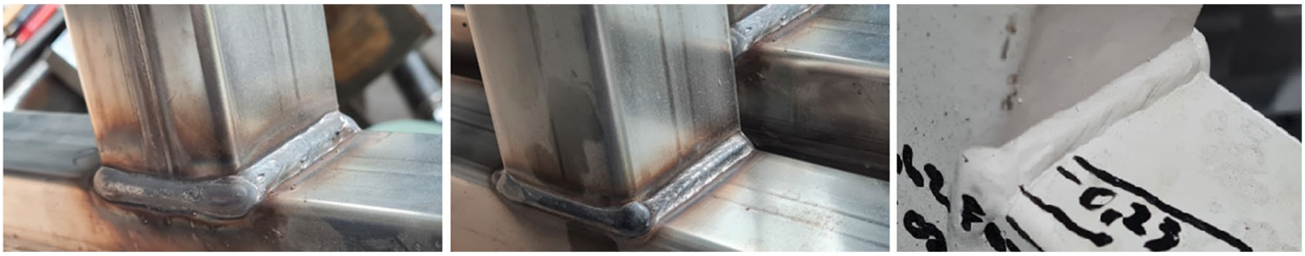

Fig. 2 Specimen 1.4678 manually welded (left) and robot welded (middle), 1.8849 (right)

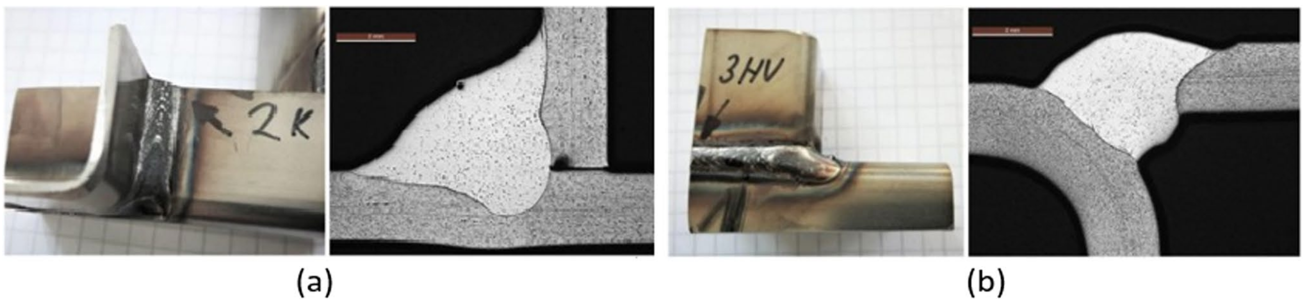

Fig. 3 Micrographs, 1.4678 at **(a)** crown position and **(b)** saddle position

rod in flat position, 165–170 A, 19 V, wire feed speed 7 m/min, welding of seam layers in horizontal position using 150–155 A, 17, 6–18 V, and wire feed speed 5 m/min. After welding the cover layers, the seams were mechanically cleaned using a wire brush.

All weld seams start and end in the corners. Because the corners also face maximum stresses for those joints, this specification is usually not recommended from the durability point of view but refers to practical aspects in manufacturing of complex bus frames. Therefore, this weld sequence was used for all specimens. See Fig. 2.

All specimens made of 1.8849 were delivered electro-coated for corrosion protection. 1.4678 specimens have been left uncoated.

Figure 3 shows examples of micrographs at two different positions of specimens made of the higher-strength material.

A typical failure pattern at the location of maximum bending moment can be seen in Fig. 4. Two crack locations can be seen. The crack started at the section corners due to the maximum structural stress at such joints and maybe additional notch effect due to the transition of two fusion lines. The crack shown in the figure shows the crack length after 0.2, 1.0, 5.0 mm increase of displacement at the load intake of the load-controlled fatigue tests. All fatigue life values as given in this paper reflect load cycles for an increment of 0.2 mm.

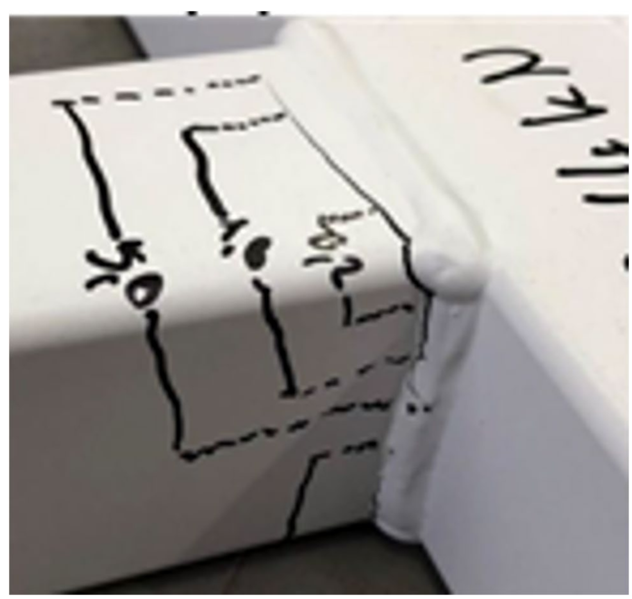

Fig. 4 Typical failure pattern and crack lengths at different displacement increases, values in mm

2.2 Test equipment

Tests were performed using a hydraulic as well as a resonance testing machine, both from Schenck. The hydraulic cylinder was selected for very short high blocks due to shorter start-up times. Longer blocks, especially at the

Table 3 Parameters of SN-curves

Material	Welding	n	$\Delta S_{2E6,50\%}$	m	T_N	$s_{lgN,corr}$
1.8849	Manual	11	124 MPa	8.42	2.8	0.18
1.4678	Manual	7	126 MPa	5.62	3.0	0.19
1.4678	Robot	16	109 MPa	6.31	5.5	0.29

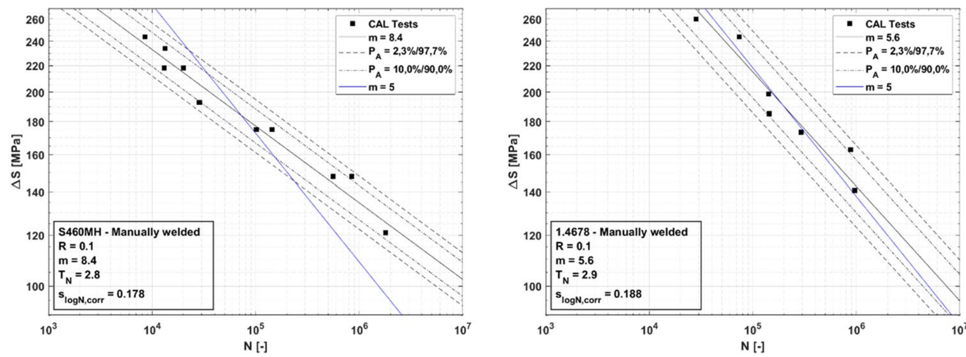

Fig. 5 SN curves, manually welded specimens, 1.8849 (left) and 1.4678 (right)

low level, were then performed with the resonance testing machine. In contrast to the hydraulic cylinder, this required about 100–300 cycles to reach the desired test level. To ensure that cycles required for start-up do not distort the calculation of the total damage or are not taken into account at all, only longer blocks were run on the resonance testing machine.

Both testing machines have a maximum test load of approx. 63 kN and are equipped with a corresponding load cell up to 63 kN. Before the tests were carried out, the load cells were calibrated to a deviation of 0.002 kN using Spider8 PC measurement electronics and a suitable calibration load cell up to 10 kN.

The test frequency of the hydraulic cylinder is in the range of approx. 5–9 Hz. The frequency of the resonance testing machine is about 12 Hz.

3 SN-curves

Using specimen from the same production lot as the later variable amplitude tests, at first, SN-curves for the structure were obtained: 12 tests of 1.8849 and 7 tests for 1.4678, both manually welded and 16 tests of 1.4678 robot welded specimen. The resulting raw data can be found in Table 13 in the Appendix. The parameters of the SN-curves are given in Table 3.

Figure 5 shows the resulting curves for both materials in manually welded condition for nominal bending stress in the critical weld section as well as the test results. Nominal stress was calculated by a linear transfer coefficient for the applied load DF of $c_N = 33.13$ MPa/kN and covers the bending stress only. Nominal stresses, at the location as given in Fig. 1, can be derived for dimensions used and a section modulus of $W = 5660$ mm^3 by

$$\Delta S = \frac{\Delta F \cdot 375\text{mm}}{2 \cdot W} = \Delta F \cdot c_N = \Delta F \cdot 33.13\frac{\text{MPa}}{\text{kN}} \quad (1)$$

Due to the large support spacing of 800 mm, transverse shear forces are about 4% of bending stress and can be neglected. Regression of the SN-curves were done using the equations from DIN 50100 [22] since the project is focused on steel construction and crane design which usually use this procedure. According to this rule, especially for small sample numbers ($n < 10$) the logarithmic standard deviation s_{lgN} tends to underestimate and must therefore be corrected according to:

$$s_{lg,N,corr} = s_{lg,N}\frac{1 - 1.74}{n - 2} \quad (2)$$

As shown in the figure, curves from regression and valid for $P_A = 2.3\%$, 10%, 50%, 90%, and 97.7% are shown in black color.

The scatter bands are reasonable low due to the use of specimens from the same production lot.

In addition to the free slope from regression, the regression line with fixed slope $m = 5$ is also shown in blue, which represents a common value for SN curves for such thin-walled welded components.

The increase of the slope exponent especially of $m = 8.4$ for 1.8849 and less pronounced by $m = 5.6$ for 1.4678 show a significant effect of the material strength of the base material as well the effect of the thin-walled welded structures in these results.

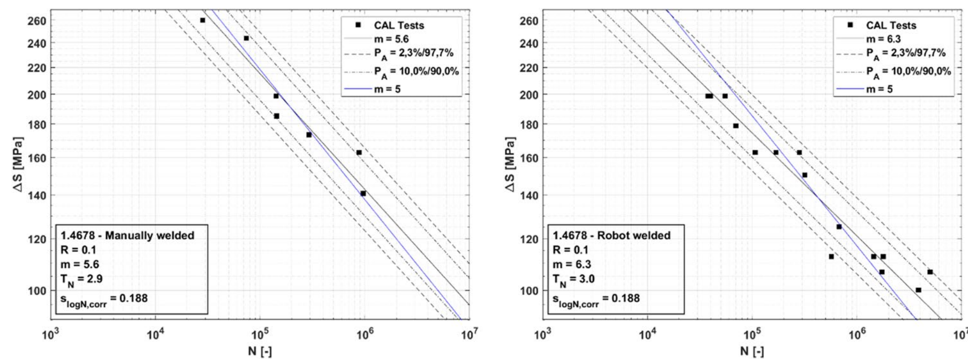

Fig. 6 SN-curves, manually welded specimens 1.4678 (left) and robot welded (right)

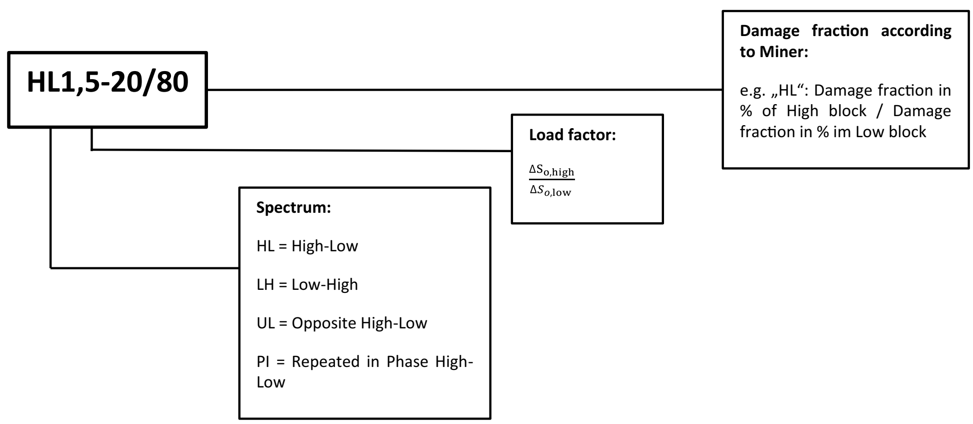

Fig. 7 Naming convention for the specimens

In Fig. 6, the difference between the manually welded and the robot welded specimens made of 1.4678 can be seen. A significant increase of the fatigue strength of the manually welded specimen compared to the robot welded ones is due to the material pile up in the highly stresses corner for the latter, which creates additional notch effect which can be seen in Fig. 2. We currently have no explanation for the lower strength, which can be seen for the robot welded specimens for very high stress ranges. Those fatigue life values should be less prone to stress concentration. Geometrical differences in the local cross section might be responsible for this effect. Using image analyzing software in order to quantify the local weld geometry could help to quantify the local notch severity. Such investigation has not been in the scope of the research project.

4 Load spectra for variable amplitude testing

The SN-curves have been taken to define the subsequent variable amplitude spectra using analytical damage accumulation by the Miner's rule. Except for reversed loading conditions, all cycles are applied using a stress ratio $R = 0.1$. For reversed loading, $R = 10$ is used for compression cycles.

1.8849 Maximum stress ranges are fixed to $\Delta S_h = 250$ MPa for all spectra which corresponds to a fatigue life according to the SN-curve from regression of 5555 cycles. This is well above 5000 cycles which defines the transitions between high and low-cycle fatigue ranges according to DIN 50100 [22]. The minimum load levels are defined by the ratio or load factor LF of upper to lower stress ranges by $LF = |\Delta S_h| / |\Delta S_l|$. The maximum load factor used was 1.8 which corresponds to a minimum stress cycle of 139 MPa and a cycle to failure of 778,243 cycles. The defined cycles thus are well within the range of the SN-curve.

1.4678 + CP700 Maximum stress ranges are fixed to $DS_h = 277$ MPa for all spectra which corresponds to a fatigue life according to the SN-curve from regression of 5405 cycles. The minimum load levels are defined by the ratio or load factor LF of upper to lower stress ranges by $LF = |\Delta S_h| / |\Delta S_l|$. The maximum load factor used was 1.8 which corresponds to a minimum stress cycle of 154 MPa and a cycle to failure of 219,578 cycles. The defined cycles thus are well within the range of the SN-curve.

For the variable amplitude testing, different spectra have been defined. The naming of the tests for variable amplitude loading was done using the naming convention according to Fig. 7.

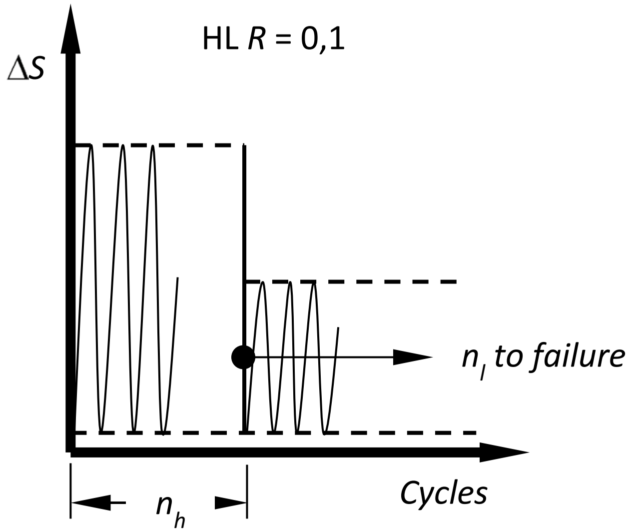

Fig. 8 High-low spectra

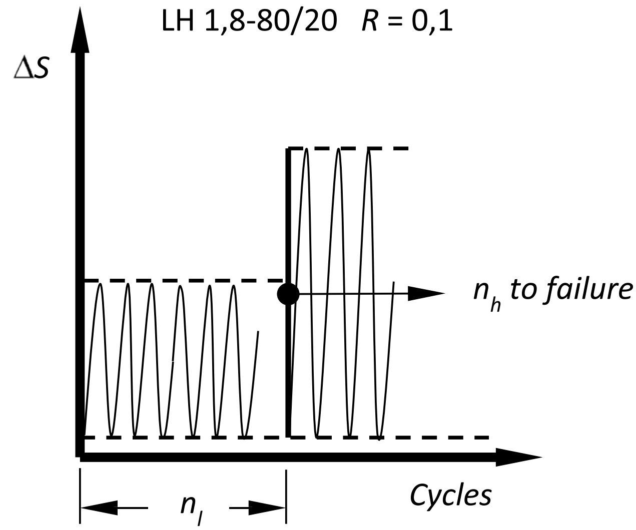

Fig. 9 Low–high spectra

Using the SN-curves the following spectra has been defined using analytical linear damage accumulation for an allowable damage of 1.0 for the respective material.

4.1 High-low spectra

The test scenarios result from a variation of the ratio of high load (overload) ΔS_h to low load (base load) ΔS_l on one hand, and from a variation of the ratios of the partial damage sums of high load D_h and low load D_l on the other hand. The damage proportions for the 4 high-low-spectra in Fig. 8 are estimated with the damage accumulation rule according to Palmgren–Miner using the SN-curves as obtained for the respective material. The maximum damage according to Palmgren–Miner of 80% due to the overload ensures that a fracture should not already occur during the initial overload block. The maximum and minimum load levels have been defined to be safely within the range of the SN-curve for high-cycle fatigue.

4.2 Low–high spectra

Using just the worst-case from the high-low spectra the levels for a reversed sequence low–high was derived. The spectrum according to Fig. 9 is resulting from this approach.

4.3 Opposite phase high-low spectrum

For transportation systems, in-phase spectrum levels are usual loading conditions, especially in the direction of the acceleration due to gravity. Therefore, those spectra have been tested with higher effort. UL1.8–80/20 test spectrum was also used to investigate overloads occurring in opposite phases as shown in Fig. 10. The R-ratio of the foregoing high-block in compression amounts $R = 10$.

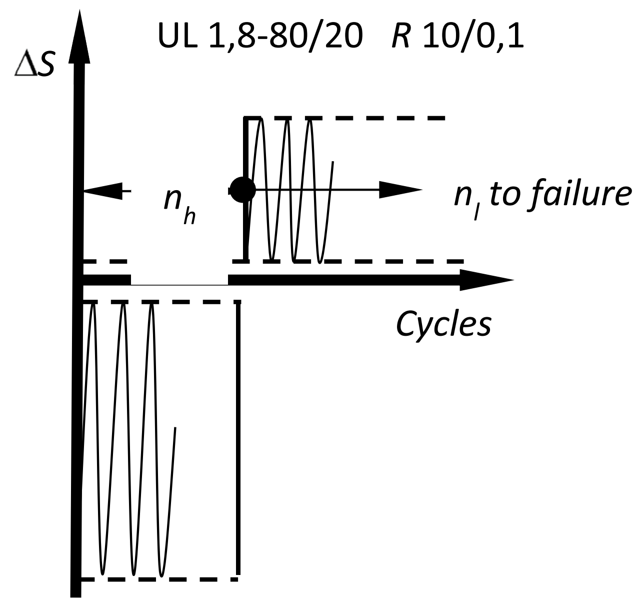

Fig. 10 Opposite phase high-low spectra

4.4 Repeated loads in-phase

Block-type spectra of repeated overloads have been defined according to Fig. 11. Each of those in-phase high-low spectra was designed for a repetition of each block 8 times to analytical failure. Such spectra represent also the occurrence of rare overloads like misuse or pot-hole driving.

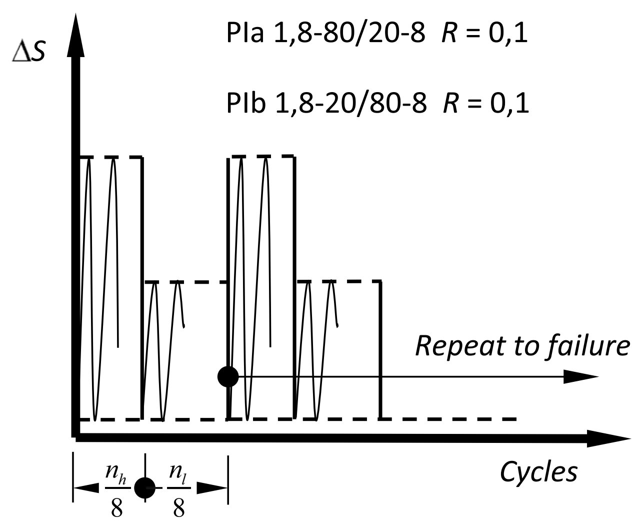

Fig. 11 Repeated in-phase high-low spectra

5 Test results from variable amplitude testing

The results from variable amplitude testing as raw data can be seen in Table 14 (1.8849) and Table 15 (1.4678) in the Appendix.

The relative Miner sums in Tables 14 and 15 given by $D_V = D_{test}/D_{calc}$ reflect the prognosis quality of the linear damage accumulation as calculated against the corresponding SN-curves. D_{calc}, which is the expected theoretical damage for sizing the spectra before testing, is 1.0 for all cases. $D_V > 1.0$ refers to an experimental damage higher than theoretically and indicates a very conservative value for using the Miner rule for such cases. Vice versa, values below 1.0 result in an underestimation of the analytical fatigue life using the Miner rule if compared to the experiments.

In the left column, those tables also contain an equivalent cycle to failure number $N_{äq}$ as calculated for a constant amplitude spectrum at the maximum stress cycle ΔS_h for the corresponding material. This reflects a Gassner-type evaluation.

Apart from the reversed loading case UL-1.8–80/20, no mean stress correction is necessary, since the two-level tests and the component SN curve were performed at the same load ratio. For UL-1.8–80/20, a correction factor for medium level[1] residual stresses of $f(R) = 1.3$ according to [24, 25] was applied for the cycle in compression. Due to the thin-walled design, this should be a reasonable assumption but need to be taken with caution. There is too little knowledge about mean stress effects of hollow sections in general. Table 14 contains both evaluations with and without the mean stress correction.

Marked in the tables are a few tests which have been identified as outliers for the test series of the respective stress spectrum. The procedure of the outlier detection was simply done by visible inspection of the test series in probability paper. An example is shown in Fig. 12 where the test marked in green is identified. Using log-normal or normal distributions for D_V does not give different results. Outliers are not contained in the regression curve to get values for different probabilities to calculate the scatter factor T from the 90% and 10% quantiles as well as the standard deviation s_{lg} according to the equation

$$s_{lg} = \frac{1}{2.56} \lg(T) \tag{3}$$

The resulting statistical values can be seen in Tables 4 and 5. Important findings are.

- High-low spectra only show outliers, but only for the manually welded 1.8849.
- Especially spectra with high damage content (80%) in the high block show more than one outlier.
- Low–high spectrum shows largest scatter.
- Median values of all relative damage sums are above 0.84 up to 1.5, all 10% values above 0.51 up to 1.0 (except UL1.8–80/20 with mean stress correction. See "Discussion" section).

The boxplots in Fig. 13 shows the dispersion of relative damage sums. Each box covers 50% of data, the black whiskers represent 1.5 times the distance between mean value (in red) and blue box boundaries. However, the whiskers are cut to the next data point inside, which is why whiskers of unequal length can also be seen. The collective form UL1,8–80/20-korr represents the damage sums calculated considering mean stress correction.

The individual points are enumerated consecutively for this purpose and match the numbering above or below the individual boxplots.

1. Test series with high partial damage at high amplitudes show less scatter.
2. Overloading in compression which theoretically should accelerate crack propagation show low scatter. For using mean stress correction or not: relative damage sum $D_V < 1$ with and without mean stress correction, thus linear damage accumulation leads very unsafe results.

[1] DVS 0905 suggest medium mean stress in cases, where zero mean stress cannot be guaranteed, thin-walled structures, no restraints of the component influencing the weld region are present. This is the case for the test as described here. With respect to mean stress correction and compared to the IIW-Recommendations, DVS 0905 is based on results from a comprehensive German research project [23] focusing on mean stress effects of welded structures and thus DVS is preferred here.

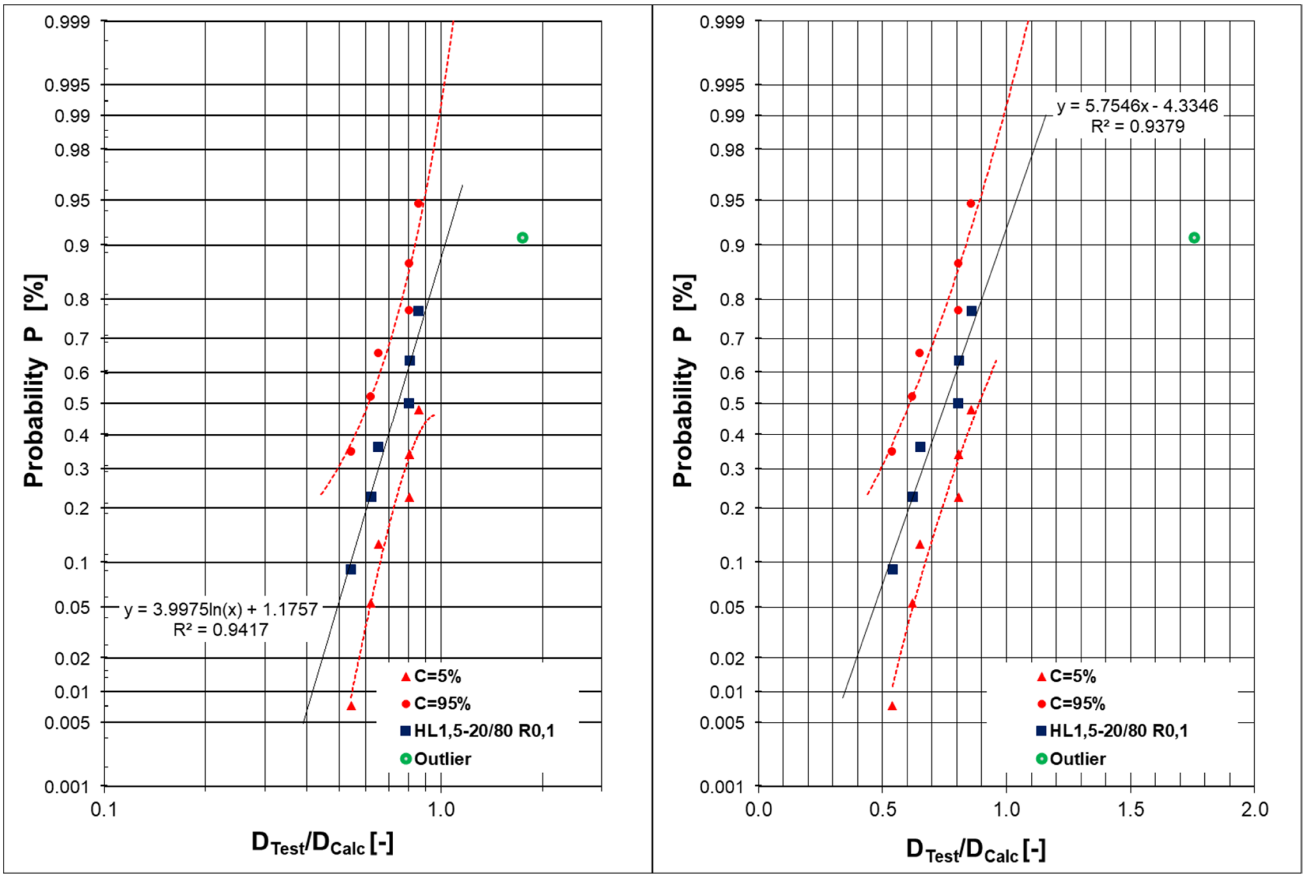

Fig. 12 Probability plots with lognormal distribution (left) and normal distribution (right), HL-1, 5–20/80, 1.8849

Table 4 Statistical evaluation of relative damage sums 1.8849

Spectrum	Samples	Outliers	T	s_{lg}	$D_{V,50\%}$	$D_{V,10\%}$	
HL1,5–20/80	7	1	1.90	0.11	**0.8**	**0.5**	
HL1.5–80/20	7	2	1.23	0.03	**1.0**	**0.9**	
HL1.8–20/80	7	1	2.34	0.14	**1.5**	**1.0**	
HL1.8–80/20	7	3	1.13	0.02	**1.1**	**1.0**	
LH1.8–20/80	7	0	2.65	0.17	**0.8**	**0.5**	
UL1.8–80/20	7	0	1.03	0.01	**0.9**	**0.8**	No mean stress correction
UL1.8–80/20	7	0	1.3	0.04	**0.1**	**0.1**	Mean stress correction
PIa1.8–80/20–8	7	0	1.73	0.09	**0.8**	**0.6**	
PIb1.8–20/80–8	4	0	2.70	0.17	**0.9**	**0.7**	

Bold values show the most significant information in the tables

Table 5 Statistical evaluation of relative damage sums 1.4678

Spectrum	Samples	Outliers	T	s_{lg}	$D_{V,50\%}$	$D_{V,10\%}$
HL1,5–80/20	7	0	2.67	0.17	**1.5**	**0.9**

Bold values show the most significant information in the tables

3. Damage prognosis tends to the unsafe side when there is higher partial damage at lower amplitudes.
4. If the damage fraction of large amplitudes increases, then scatter is reduced.

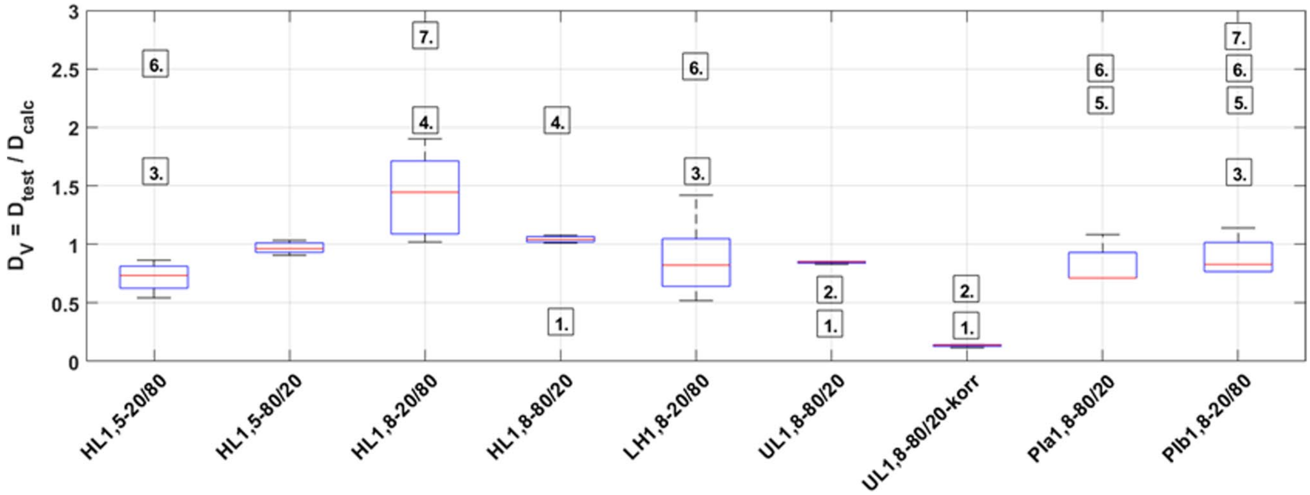

Fig. 13 Relative damage sums in boxplot without outliers (censored), 1.8849

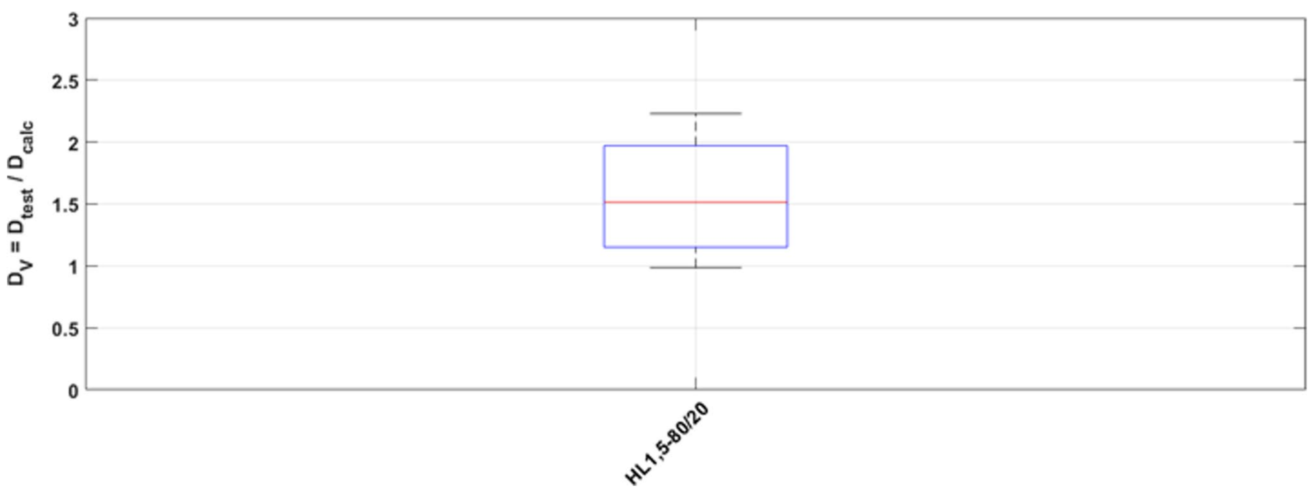

Fig. 14 Relative damage sums in boxplot, 1.4678 (robot welded)

5. In repetitive block programs there are hardly any differences in the distribution of the partial damages of the two load levels.
6. High content of cycles in the low load range leads to an unsafe evaluation.
7. High overloads in the high-low spectra theoretically leads to deceleration of cracks, which can be seen in high relative damage sums. Rare overloads at the very beginning for this sequence type has a larger effect towards underestimating life than repeated high-low blocks.

Figure 14 shows the damage totals of the test series HL1.5–80/20 of the high-strength steel 1.4678. In direct comparison with the same test series for the material 1.8849, it is noticeable that the linear damage accumulation leads to a more conservative result. In the median, the total of the individual tests is $D_V = 1.5$.

6 Residual stress measurement

To get first impression about residual stresses, measurements have been taken on one specimen of 1.4678. Since the samples made of 1.8849 have all been electrocoated, residual stress measurements could not be performed for those. A proper removal of the electrocoat was not possible.

For measurement, X-ray diffraction was used. See parameters in Table 6. This work was performed by University Kassel, Germany. The following distributions show stresses

Table 6 Data and parameters for X-ray diffraction

Measuring device	Pulstec µX360s
Radiation type	CrKb radiation
Tube voltage	20 kV
Tube current	1.5 mA
Collimator	1 mm
Measured lattice plane	311 plane
Angle of attack	30°
Evaluation range	2Q = 125°–150°
Lattice constant	D = 3.5920 A
Modulus of elasticity	E = 193,000 MPa
Poisson's ratio	n = 0.3

in lateral and longitudinal direction of the horizontal tube. Path coordinates can be taken from Fig. 15. The paths in the following figures are along the horizontal tube in web center and tube edge through the weld and 150 mm away from the weld along a lateral path on the web. Since the TWIP steel was hardened by cold forming, stresses at the remote position 150 mm away from the weld and HAZ were also taken.

Longitudinal and transverse residual stresses measured at this distance over the transverse section can be taken from Fig. 16. Both the longitudinal and the transverse residual stresses seem to be distributed relatively constant over the transverse section and change only in the edge areas shortly before the beginning of the bending radii of the tube, which

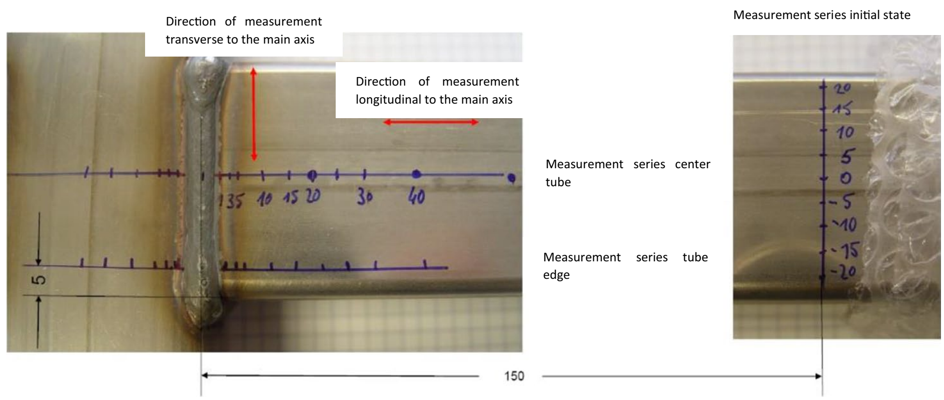

Fig. 15 Longitudinal and transverse coordinates on the web of the horizontal tube

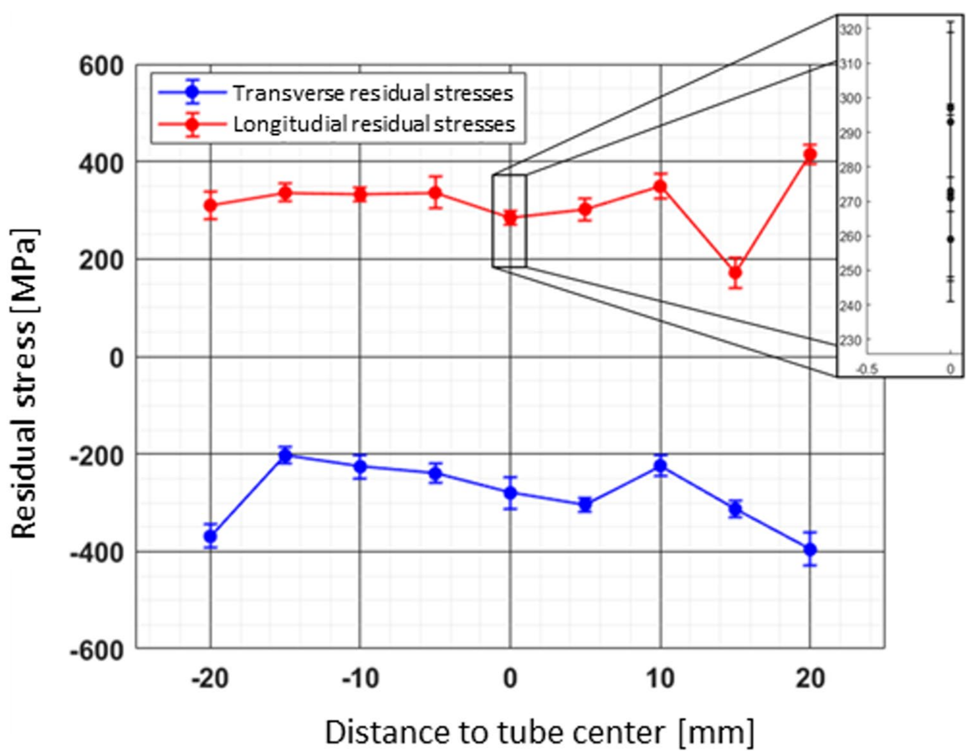

Fig. 16 Residual stresses in 150-mm distance to weld, measurement series initial state

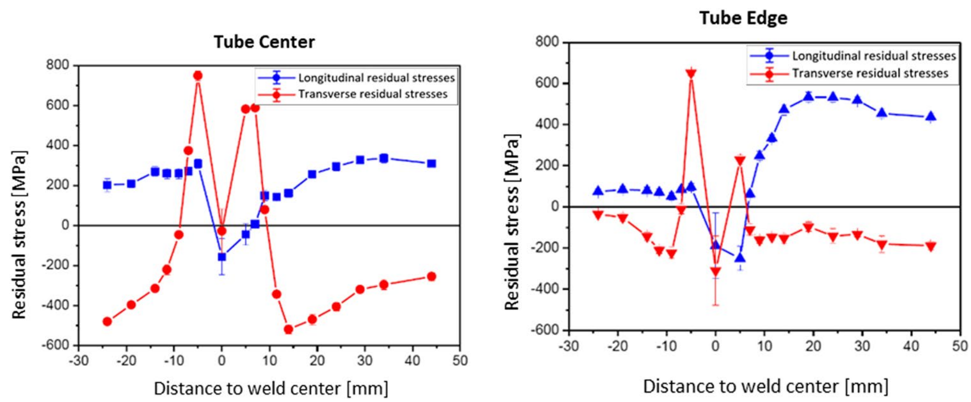

Fig. 17 Residual stresses through weld along web center (left) and along tube edge (right)

suggests that the residual stress state is influenced by the bending process. The longitudinal residual stresses are in the tensile range, whereas the transverse residual stresses are in the compressive range. Both stress components are of significant magnitude. However, the repeat measurements performed without repositioning in the center of the tube, cf. Figure 16—enlarged section, show certain scatter which was also found to be similar in magnitude in all other measurements. However, a reproducibility of the results with such scatter could be proven by several repeat measurements.

The measurements at weld position carried out in the center of the tube and at the edges show a clear influence on the residual stress distribution compared to areas without heat influence. Figure 17 (left) shows the longitudinal and transverse residual stress distribution along the medial line of the web and Fig. 17 (right) along the path along the edge of the section. The influence of the weld is shown by a clear shift and sign change of the residual stresses in both the longitudinal and transverse residual stresses in the weld zone. Since the residual stresses were measured both on the right and on the left of the weld seam, these curves differ due to the different positions of the respective tubes. Nevertheless, it can be observed that higher tensile residual stresses occur in the longitudinal direction in the edge region of the tubes than in the center of the tube. This observation also agrees with the measurements far away from the HAZ. Similar findings can be obtained when considering the transverse residual stresses. Here, however, in agreement with the measurements in the unaffected zone, the residual stresses are in the compression. In summary, it can be stated that the heat input from the welding process only affects the residual stresses in the immediate vicinity of the weld seam.

7 Stress concentration factors

Finite element analysis is state of the art for analytical assessment of deformation, stresses, and strains also for welded structures [26]. Besides the experiments, notch factors to evaluate structural and notch stresses were determined for the geometry of the thin-walled square hollow joint by finite element analysis in this project as well. Using those stress concentration factors, the SN-curves based on nominal stresses can be transferred to structural stresses and effective notch stresses. For finite element analysis, ANSYS Workbench 2021 R2[2] was used.

Structural stresses are derived by linear and quadratic extrapolation according to the IIW Recommendations [27], effective notch stresses based on a fictitious radius in the notch root and weld toe of $r = 0{,}3$ mm as suggested by the DVS 0905 [25]. For such thin-walled structures the reference radii 1.0 mm as suggested by [27] weakens the weld throat too much and should not be used. Therefore, this reference radius should not be used for this structure.

The nominal dimensions of the tubular joint as described in chapter 2 have been used to model the geometry. Due to symmetry, 1/4 of the total structure was modeling applying symmetry boundary conditions. At the bearing rolls, the structure is simply supported. Loading is applied by the compressive force on the top face of the vertical tube.

To reduce computational effort, submodeling was used. The domain of the submodel can be seen in Fig. 18 (right). This model included the stiffening effect of the weld seam with angular, i.e., discontinuous transitions for the analysis of structural stresses and in case of notch stress analysis the fictitious radii at weld root and weld toe. The flank angle is set to 45° (Fig. 19).

Only solid elements with quadratic shape functions have been used. For mesh refinement in weld root and weld toes for the effective notch stress concept, the DVS 0905 code of practice recommends at least 24 elements along a 360° arc in the notch radius and also the corresponding element edge length normal to the notch surface for quadratic approach functions of the finite elements. A convergence study on our model confirms this recommendation as seen in Fig. 20 (right).

[2] ANSYS is trademark of ANSYS, Inc., Canonsburg, PA, USA.

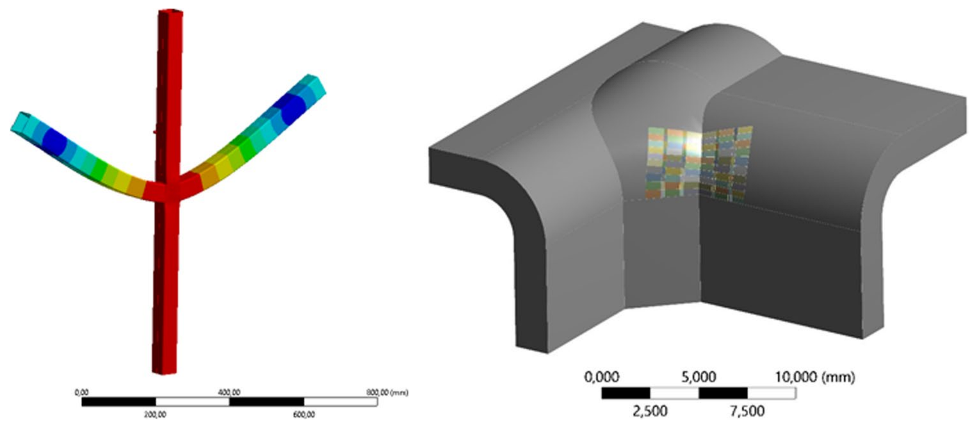

Fig. 18 Displacement under loading (left), submodel domain (right)

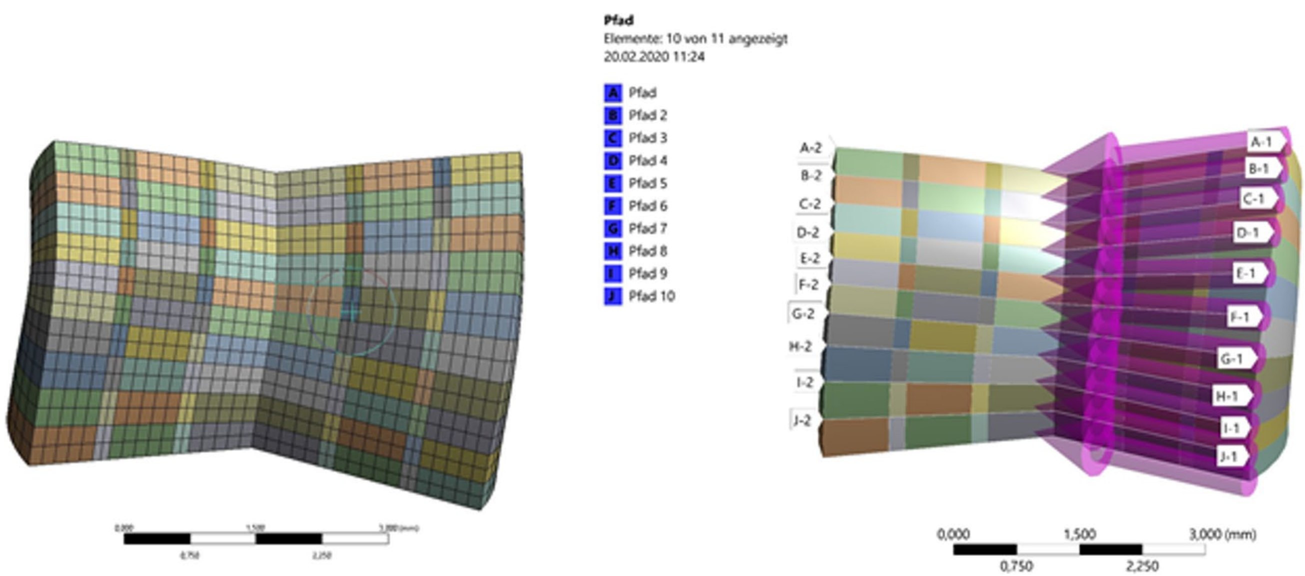

Fig. 19 Mesh detail in maximum stressed zone (left), path definitions for structural stress extrapolation (right)

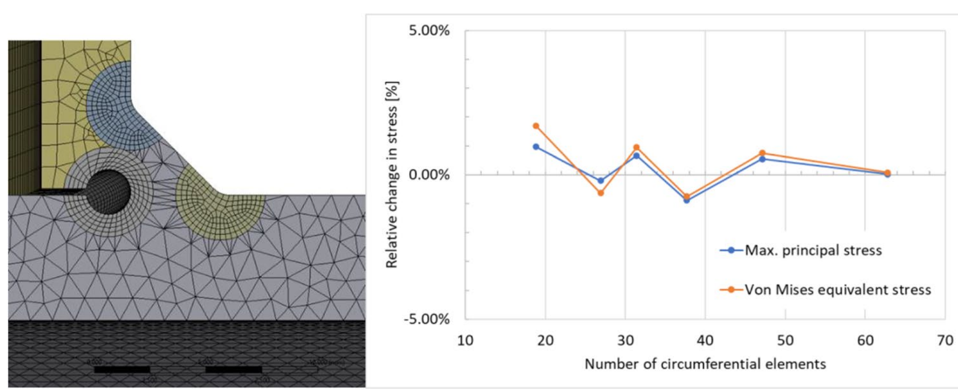

Fig. 20 Mesh detail of root and weld toes (left), convergence behavior of mesh refinement (right)

To determine the structural stresses, the methods according to Haibach (1 mm and 2 mm stresses) [], as well as the linear and quadratic extrapolation methods according to [27], were applied. For this purpose, the notch area was modeled without filleting the seam runout. To determine the stress curves, the required evaluation points were defined by means of several evaluation paths and sections perpendicular to the notch on the component surface, see Fig. 19 (right). The path with the highest resulting stress was used for further evaluation. See

Fig. 21 Structural stress evaluation for path with maximum principal structural stress

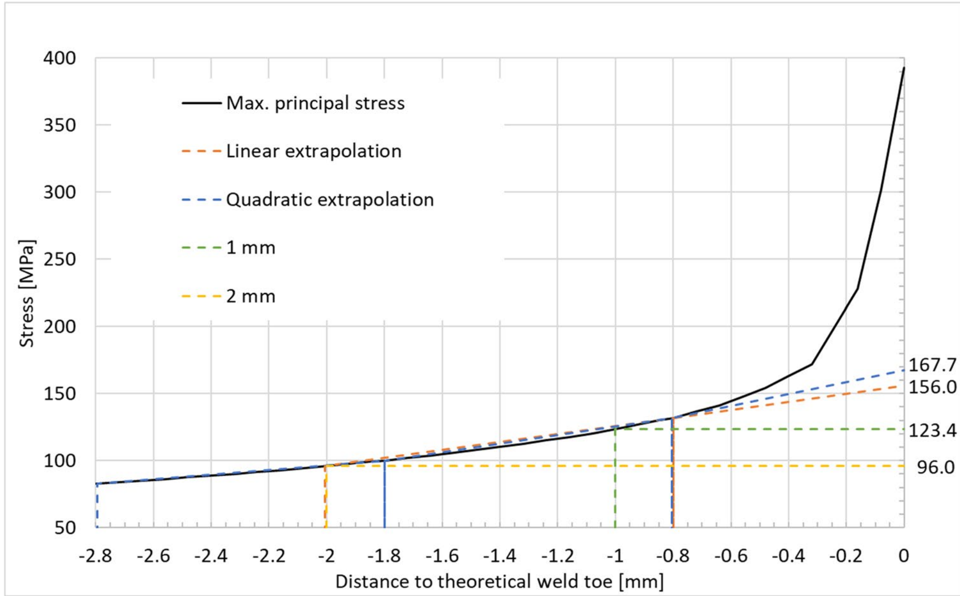

Fig. 22 Notch stress distribution, maximum principal structural stress and at the weld toe of maximum stress

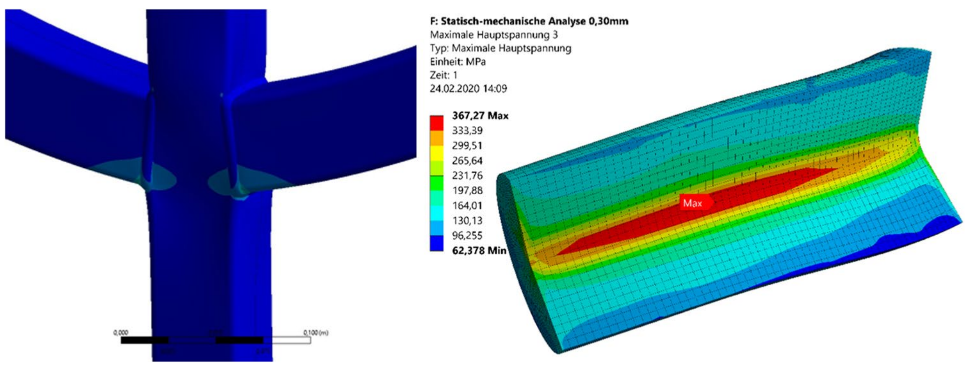

Table 7 Stress concentration factors, SCF

$K_{t,hs,1mm}$	$K_{t,hs,2mm}$	$K_{t,hs,lin}$	$K_{t,hs,quad}$	$K_{t,0.30mm}$
3.73	2.90	4.71	5.06	11.09

Fig. 21, showing the maximum principal stress ending at the hot spot along the tube flange in tension. The structural stress values can be seen at the right.

It can be seen from this figure that the Haibach structural stress underestimates very much and thus this definition cannot be taken for such thin-walled structures. This pragmatic method performs much better for thicker welds.

Notch stress analysis results in maximum stresses in the weld toe at the section corners only.

Stresses in the weld root are approximately a factor of 4 lower than at the location of maximum weld toe. Therefore, they can be excluded as failure critical locations. This was also confirmed in the tests with the same geometry for both materials.

Stress concentration factors SCF represent the ratio between the determined structural or notch stresses and the previously defined nominal stresses (Fig. 22). Nominal, structural, and notch stress concepts always refer to linear-elastically determined stresses. For this reason, structural and notch stresses can be obtained simply by linear scaling as shown in Table 7.

$$K_t = \frac{\sigma_k \text{ or } \sigma_{hs}}{S} \tag{4}$$

The SCF derived for the two Haibach methods show the strong underestimation of the structural stress method for such thin-walled structures. For stress fields showing nonlinear distributions in front of the hot spot the quadratic extrapolation should be used for hot-spot stress evaluation.

According to DVS 0905 [25, 28], checking against a SN curve for the base material in addition to the check with respect to the SN curve according to the FAT class is mandatory for mild notches having low stress concentration factors. To exclude such cases, minimum values of the seam shape

Table 8 Structural stress concept, characteristic values for 2E6 cycles

	Experiment			IIW recommendations		
	$\Delta S_{2E6,50\%}$	m	$K_t \cdot \Delta S_{2E6,50\%}$	FAT	$\Delta\sigma_{hs,2E6}$	m_{DVS}
1.8849 manually welded	124 MPa	8.42	**627**	90	**126**	5
1.4678 manually welded	126 MPa	5.62	**638**	90	**126**	5
1.4678 robot welded	109 MPa	6.31	**552**	90	**126**	5

Bold values show the most significant information in the tables

Table 9 Effective notch stress concept, characteristic values for 2E6 cycles

	Experiment			DVS 0905		
	$\Delta S_{2E6,50\%}$	m	$K_t \cdot \Delta S_{2E6,50\%}$	FAT_{Toe}	$\Delta\sigma_{k,2E6}$	m_{DVS}
1.8849 manually welded	124 MPa	8.42	**1375**	300	**420**	5
1.4678 manually welded	126 MPa	5.62	**1397**	300	**420**	5
1.4678 robot welded	109 MPa	6.31	**1209**	300	**420**	5

Bold values show the most significant information in the tables

Table 10 Structural stress concept, comparison of characteristic values

	IIW recommendations		Experiment			
	$\Delta\sigma_{hs,1E4}$	$\Delta\sigma_{hs,2E6}$	$K_t \cdot \Delta S_{1E4,50\%}$	$K_t \cdot \Delta S_{2E6,50\%}$	SR_{1E4}	SR_{2E6}
1.8849 manually welded	364	126	1176	627	**3.2**	**5.0**
1.4678 manually welded	364	126	1638	638	**4.5**	**5.1**
1.4678 robot welded	364	126	1287	552	**3.5**	**4.4**

Bold values show the most significant information in the tables

factor K_w must be achieved, which is defined by the ratio of notch stress to structural stress and is depending on the reference radius. The minimum value of K_w for $r = 0.3$ mm to use the FAT class-based SN curve for the fatigue assessment only is $K_{w,min} = 2.13$ [25]. In our case, the ratio from finite element analysis gives $K_w = 2.19$ which is close but larger. The small distance from the limit in this use case with a high localized stress concentration and flank angle of 45° is remarkable.

8 Discussion

8.1 Constant amplitude testing

First, the SN curves are compared to FAT classes taken from DVS 0905 for the effective notch stress concept and from the IIW recommendations for structural stresses, both applied to maximum principal stress. For load carrying welds, FAT90 is recommended for structural stresses and FAT300 is recommended for $r = 0.3$ mm for the effective notch stress concept, both using a slope exponent of $m = 5$ for thin-walled structures.

FAT classes are given for a low probability of failure as typical in many standards of 2.3% (about equal to a probability of survival of 95% of the mean together with either a two-sided 75% or a one-sided 95% confidence limit or alternatively mean minus two times standard deviation [27]). Transferring the FAT classes to a failure probability of 50%, multiplication by 1.3 as a pragmatic approach is used. IIW recommendations suggest a value of less than 2.3 for the number of specimens to obtain the SN-curve. Also, FAT classes are valid for a stress ratio $R = 0.5$. According to DVS 0905 [25], transformation to $R = 0.1$ requires an additional factor $f(R) = 1.073$ in the case of conservatively assuming residual stresses. We consider this value as a theoretical upper bound when looking on the residual stresses for the TWIP steel as seen in Fig. 17 (right). For comparison of the most probable mean values from regression $\Delta S_{2E6,50\%}$, the FAT class in total needs to be multiplied by an assumed 1.4 to obtain comparable characteristic values. We consider this as an upper bound value for the code-based SN data for 50% probability. The modified FAT classes and the stress ranges from constant amplitude testing multiplied by the corresponding stress concentration factors can be seen in Table 8 for characteristic values of structural stress $\Delta\sigma_{hs,2E6}$ and Table 9 for the effective notch stresses $\Delta\sigma_{ns,2E6}$, both valid for a probability of 50%. A significant difference can be seen in both tables. For structural stresses, the stress concentration factor from quadratic extrapolation only is used for this evaluation.

To get a better view on the full range of the SN-curves, the ratios of characteristic values can be seen in Tables 10 and 11. The values for 10^4 cycles have been calculated using the respective slope exponents for each approach from Tables 8 and 9. Also, the K_t-values are applied with the same magnitudes as for $2 \cdot 10^6$ cycles. The ratios between characteristic values from the experimental

Table 11 Effective notch stress concept, comparison of characteristic values

	DVS 0905		Experiment			
	$\Delta\sigma_{k,1E4}$	$\Delta\sigma_{k,2E6}$	$K_t \cdot \Delta S_{1E4,50\%}$	$K_t \cdot \Delta S_{2E6,50\%}$	SR_{1E4}	SR_{2E6}
1.8849 manually welded	1212	420	2580	1375	**2.1**	**3.3**
1.4678 manually welded	1212	420	3586	1397	**3.0**	**3.3**
1.4678 robot welded	1212	420	2723	1176	**2.3**	**2.8**

Bold values show the most significant information in the tablesf

SN-curves and the code-based values are given for 10^4 and $2 \cdot 10^6$ cycles in the last two columns of these tables.

The results demonstrate a massive increased fatigue strength of for both materials and both welding processes if we compare the data to the transferred FAT classes and standardized slope exponents from the codes. This gives an indication that — due to high-strength material, thin-walled structures and tested components, not just weld details — the application of the cited technical recommendations is much too conservative for such cases.

The higher difference in strength between experiment and code-based strength by using the structural stress is even higher compared to the notch stresses. Because the experimental obtained characteristic values are based on the same nominal stress but different stress concentration factors, this difference can only be due to one or two wrong FAT classes. The FAT classes from IIW recommendations apply to any load-carrying weld geometry and thus those FAT values might be more conservative than the corresponding FAT class for the effective notch stress concept. A single master SN-curve is used by the effective stress concept as well, but very local stress concentrations at the critical section corners are captured by this concept only. We assume, this might be the reason for this difference.

Since the increase of the strength of the manually welded specimens for both materials are about the same for the lower stress ranges, the strength increase at $2 \cdot 10^6$ cycles might be less due to the material but the high stress concentration of a component type structure and the thin-walled dimensions.

The strength increase of the TWIP steel is much more significant for 10^4 cycles though. This reflects the higher monotonic material strength of this advanced steel. The TWIP-steel has a steeper SN-curve due to the higher strength for monotonic loading.

The results from the constant amplitude testing have shown that by using the TWIP steel, not only massive weight reductions for monotonic loadings but also for variable amplitude loading can be achieved for such structures. The higher the loads of rare events or the higher the maximum stress of an applied spectrum loading, the higher the advantage of the TWIP steel.

8.2 Variable amplitude loading

Tests for CAL and VAL were all done using specimens of the same lot to apply the SN-curves on life estimation with reasonable accuracy. Although each of the variable amplitude spectra have been repeated seven times for most of the spectra defined, the resulting data can only give an indication of tendencies. A final conclusion for an improvement of the linear damage accumulation cannot be drawn by these tests alone.

The variable amplitude spectra as defined in chapter 4 and resulting relative damage sums D_V in chapter 5 based on the raw data in Tables 14 and 15 in the Appendix. The resulting statistical values can be seen in Tables 4 and 5. Important findings are as follows.

The effects as observed by fracture mechanics on speed up or slow down of crack propagation due to varying mean stress and varying amplitudes in two-step loadings [29] can be seen for the fatigue of welded specimens investigated here as well. Change from high to low in phase slows down crack propagation temporarily and speeds up from low to high stress cycles. Change from negative high stress cycles to positive low ones (reversed mean stress) also yields a speed up. This can be seen in the experimental results obtained. Since the linear damage accumulation does not consider those physical based sequence effects, this — besides other reasons — is reflected by the relative damage sums $D_V > 1.0$ or $D_V < 1.0$.

Median values of all relative damage sums (except UL1.8–80/20 with mean stress correction, see below) are in general well above 0.84 up to 1.5, all 10% values are above 0.51 up to 1.0.

Having a larger fraction of damage at low stress cycles compared to the large stress cycles increases scatter. This is comparable to the different scattering behavior of SN-curves at high and low load amplitudes. Vice versa, spectra with high damage content for large stress ranges show lower scatter of the estimated life by liner damage accumulation.

IIW recommendations [27] suggest a critical damage sum of 0.2 for fluctuating mean stresses. As can be seen in Tables 4 and 5, this criterion is fulfilled by all tests performed. Median relative damage sums of most of the tests performed are safely above 0.5. However, it is difficult to

Table 12 Fatigue life evaluation using ISO 14347

	$\Delta S_{2E6,50\%}$	m_{test}	$N_{ISO,50\%}$	m_{ISO}	$D_{V,1}$	$N_{ISO,50\%,R0.1}$	$D_{V,2}$	$N_{ISO,2.3\%}$	$D_{V,3}$
1.8849	124	8.42	358,114	3.6	5.6	590,828	3.4	139,907	14.3
1.4678	109	6.31	554,198	3.6	3.6	914,334	2.2	216,512	9.2

differentiate the load sequences to be used for this purpose. In the case of in-phase tensional loadings, i.e., mean stress remains positive for all stress ranges, the critical damage sum could be modified to higher values. An allowable value of 0.5 seems reasonable as recommended by DVS 0905 [25]. If the load spectra comply with the ones used in this program, even higher values could be taken but require additional tests for qualification.

In the following, a few more comments about the specific spectra are summarized.

8.3 High-low spectra

Trivial but referred to for plausibility: with a lower load factor LF = 1.5, the low stress level following the high level is higher as compared to $LF = 1.8$. Accordingly, the tests break down earlier than with a load factor of 1.8. Also, a theoretical damage fraction of $D_h = 80\%$ in the high block leads to earlier failure compared to setting $D_h = 20\%$.

Scatter for high-low spectra increases for a high amount of partial damage for low stress ranges. It is largest for spectra having 80% damage for the minimum stress ranges at low level.

The high-low spectrum (HL1.5–80/20) applied to specimens made of TWIP steel (robot welded) yields significant higher underestimation of fatigue life compared to the mild steel (manually welded).

8.4 Low–high spectra

The visible theoretical overestimation of life can be explained by the speed up of crack propagation for simple step loading on crack type specimens.

8.5 Opposite phase high-low spectrum

This spectrum yields a remarkable low scatter of life even though 7 specimens have been tested. Even without mean stress correction, the relative damage sum for median of $D_V = 0.9$.

UL1.8–80/20 with mean stress correction for medium level residual stresses in the welds to calculate the relative damage sum D_V leads to the worst case for the relative damage sum $D_V = 0.1$ for all spectra tested in the program. Under these assumptions, the theoretical linear damage accumulation is overestimating fatigue life significantly. Speed up of the crack propagation for this load sequence not considered in the linear damage accumulation on one hand and a mean stress correction differing from the recommendations might explain this. Therefore, this correction seems not to be valid for this type of structure. This effect requires more comprehensive tests on the effect of mean stress on this type of component like structures.

8.6 Repeated loads in-phase

The visible theoretical overestimation of life can be explained by the speed up of crack propagation for simple step loading from low to high levels on crack type specimens. This effect seems not to be compensated by the slowdown of crack propagation vice versa for repeated block loading. Compared to the tested simple two-step loadings high-low and low–high the scatter is smaller and the prognosis quality better for such block loadings.

The two block program test series do not show big differences for the two damage ratios D_h and D_l defining the spectra. Mixing the high and low stress cycles instead of two-step loading increases the damage. This correlates with observations for block loading vs. random loading [17].

9 Plausibility checks according to ISO 14347

ISO 14347 [30] is a specific standard for the design of joints made of welded hollow section. Although this code is limited to a minimum of 4 mm, it was used to check plausibility of the experimental results from constant amplitude testing. Based on the stress resultants acting on each branch of a welded joint, this method uses stress concentration factors for many different designs to estimate fatigue life as a structural stress concept at different critical positions along the welds. ISO 14347 provides SN-curves with different "FAT classes" and different slope exponents m_{ISO} dependent on the wall thickness of the tubes.

Table 12 summarizes the results for comparing the experimentally obtained life for the characteristic values at $2 \cdot 10^6$ cycles and 50% probability, $\Delta S_{2E6,50\%}$. Remarkable are the still highly different slope exponents m_{ISO} and m_{Exp}. The following check thus is only valid for the stress range used. Due to the steeper SN-curves of the ISO, the results for higher stress ranges are different.

The fatigue strength as given in ISO 14347 are valid for low failure probability. For comparison with the mean values from the constant amplitude testing, a factor of 1.3 was applied also for this analysis. $D_{V,1}$ relates the $2{\cdot}10^6$ cycles from the experimental tests to the cycle to failure number as obtained using the modified characteristic value from the ISO. A high additional safety distance of about a magnitude in life for these materials and wall thickness can be observed for this stress level. Since ISO is not focusing on high-strength steels either, this might be an additional reason for this result.

No factor of mean stress correction is included in $D_{V,1}$, because ISO 14347 does not contain a procedure for it. $D_{V,2}$ gives an idea about this effect by using an assumed correction factor of 1.15 to increase the fatigue strength towards $R=0.1$. Looking at the different results from $D_{V,1}$ and $D_{V,2}$ a potential for improving the ISO by adding a correction function for mean stress effects can be concluded.

Finally, the ISO is also checked with the given SN-curves taken from this code without modification, i.e., low failure probability and no mean stress correction. $D_{V,3}$ represents this number.

Because the fatigue strength of the manually welded TWIP steel joints is about the same as for 1.8849, this analysis is restricted to manually welded mild steel and robot welded TWIP steel only.

10 Conclusions

Welded thin-walled X-type square hollow section joints (50×50×2) made of a manually welded low alloy mild steel 1.8849 (S460MH) and robot/manually welded high strength/high ductility TWIP steel 1.4678 in cold hardened condition have been tested under bending loading with a stress ratio $R=0.1$. SN-curves as well as fatigue lives for different two-step variable amplitude spectra were obtained by the experiments. A comparison of manually and robot welded specimens has been drawn based on the interest of participation industry partners. All raw test data can be found in the appendix.

Fatigue strength of the fully austenitic TWIP steel joints in robot welded condition at $2{\cdot}10^6$ cycles is about 12% less than for the mild steel manually welded. The SN-curve is steeper thus which leads to higher strength for higher stress ranges towards LCF. The fatigue strength of the manually welded TWIP specimens is about the same as of the mild steel specimens at $2{\cdot}10^6$ cycles but they yield a steeper slope leading to a higher fatigue strength for high stress cycles. For lightweight constructions this material bears improved strength and ductility not only for static loading or plastic collapse but also for fatigue strength. These first results for $R=0.1$ indicate the lightweight potential of this new material.

Finite element analyses have been performed to calculate stress concentration factors of the components for structural and notch stress concept. Applying those stress concentration factors to FAT values from the IIW recommendations and DVS 0905 gave a significant underestimation of the code-based fatigue strengths. The difference is higher for the structural concept. Thin-walled design and component characteristics by a strong local stress concentration in the welds at the section corners might be responsible, that the two stress-based concepts differ.

Variable amplitude testing was done for different two-level block spectra. Those spectra have been designed for a total damage sum of $D=1.0$ using the experimental obtained SN-curves and a maximum stress cycle yielding about 5500 cycles on the SN-curve of the material used. A maximum factor between minimum and maximum stress cycle of 1.8 was selected. High-low, low–high, reversed high-low, and high-low sequences with 8 blocks have been tested using different fractions of partial damage for the high and the low blocks. Constant and variable amplitude testing was performed for specimens taken from the same manufacturing lots. The effects obtained from the experiments thus can be considered as of high quality. Most of the test have been performed using 7 specimens for statistical purpose. The results are on a sound basis but will require further tests on different materials, test scenarios to get enough data to improve rules for damage accumulation. Alternatively, such high experimental effort could be reduced by combining experimental with high level analytical means based on computational fracture mechanics. From the results obtained the following findings can be summarized:

- DVS 0905 recommends not to exceed a partial damage sum of 0.5 for variable amplitude loading. This is fulfilled by all tests except the case with reversed mean stresses and considering this mean stress effect.
- IIW-recommendations suggest a critical damage sum of 0.2 for fluctuating mean stresses. As can be seen in Tables 4 and 5, these recommendations are fulfilled by all tests performed.
- Median relative damage sums of most of the tests performed are above 1.0. However, it is difficult to differentiate the load sequences to be used for this purpose.
- In case of in-phase tensional loadings, i.e., mean stress remains positive for all stress ranges, the critical damage sum could be modified to higher values. A value of 0.5 seems reasonable.
- If the load spectra comply with the ones used in this program, even higher values could be taken but require additional tests for qualification.

This paper covers a contribution to a database of tests on welded hollow sections using constant amplitude testing and variable amplitude testing using different block-type spectra. It has been demonstrated, that applying selected codes leads highly safe results for the SN curves of the welded hollow sections and materials tested. Further research and modification of the technical rules is recommended.

Appendix

Table 13 Test results SN curves

	No	R	ΔS	N
1.8849 manually welded	1	0.1	175	102,000
	2	0.1	175	143,552
	3	0.1	121	361,116
	4	0.1	121	1,801,622
	5	0.1	193	28,993
	6	0.1	193	28,294
	7	0.1	218	13,013
	8	0.1	218	20,003
	9	0.1	148	849,038
	10	0.1	148	559,261
	11	0.1	244	8,495
	12	0.1	234	13,337
1.4678 manually welded	1	0.1	244	73,988
	2	0.1	163	878,269
	3	0.1	199	141,476
	4	0.1	185	143,023
	5	0.1	260	28,253
	6	0.1	173	292,746
	7	0.1	141	957,735
1.4678 robot welded	1	0.1	163	107,064
	2	0.1	100	3,856,042
	3	0.1	125	673,374
	4	0.1	150	318,023
	5	0.1	113	570,091
	6	0.1	163	168,473
	7	0.1	100	3,871,452
	8	0.1	107	1,726,437
	9	0.1	107	4,977,524
	10	0.1	163	281,609
	11	0.1	179	69,469
	12	0.1	199	37,567
	13	0.1	199	40,169
	14	0.1	113	1,449,369
	15	0.1	199	55,105
	16	0.1	113	1,768,325

Table 14 Test results variable amplitude testing for 1.8849

1.8849											
Spectrum type	ΔS_h [MPa]	ΔS_l [MPa]	$n_{h,spec}$ [−]	$n_{l,spec}$ [−]	n_{spec} [−]	$n_{h,test}$ [−]	$n_{l,test}$ [−]	n_{test} [−]	D_V [−]	$N_{äq}$ [−]	
HL1,5–20/80	250	167	1095	133,036	134,130	1095	56,633	57,728	0.54	2958	
	250	167	1095	133,036	134,130	1095	75,241	76,336	0.65	3571	
	250	167	1095	133,036	134,130	1095	259,104	260,199	1.76	9621	Outlier
	250	167	1095	133,036	134,130	1095	109,590	110,685	0.86	4701	
	250	167	1095	133,036	134,130	1095	101,143	102,238	0.81	4423	
	250	167	1095	133,036	134,130	1095	70,135	71,230	0.62	3403	
	250	167	1095	133,036	134,130	1095	100,687	101,782	0.81	4408	
HL1,5–50/50	250	167	2736	83,147	85,884	2736	94,663	97,399	1.07	5852	
	250	167	2736	83,147	85,884	2736	103,237	105,973	1.12	6,134	
HL1,5–80/20	250	167	4378	33,259	37,637	4378	38,218	42,596	1.03	5636	
	250	167	4378	33,259	37,637	4378	33,722	38,100	1.00	5488	
	250	167	4,378	33,259	37,637	4378	26,691	31,069	0.96	5256	
	250	167	4378	33,259	37,637	4378	17,645	22,023	0.91	4959	
	250	167	4378	33,259	37,637	4378	143,001	147,379	1.66	9084	Outlier
	250	167	4378	33,259	37,637	4378	118,267	122,645	1.51	8270	Outlier
	250	167	4378	33,259	37,637	4378	22,765	27,143	0.94	5127	
HL1,8–20/80	250	139	1095	617,553	618,648	1095	1,161,529	1,162,624	1.70	9329	
	250	139	1095	617,553	618,648	1095	2,106,231	2,107,326	2.93	16,026	Outlier
	250	139	1095	617,553	618,648	1095	682,211	683,306	1.08	5931	
	250	139	1095	617,553	618,648	1095	628,499	629,594	1.01	5550	
	250	139	1095	617,553	618,648	1095	906,599	907,694	1.37	7522	
	250	139	1095	617,553	618,648	1095	1,306,918	1,308,013	1.89	10,360	
	250	139	1095	617,553	618,648	1095	1,006,382	1,007,477	1.50	8229	
HL1,8–50/50	250	139	2736	385,971	388,707	2736	342,950	345,686	0.94	5168	
	250	139	2736	385,971	388,707	2736	1,456,149	1,458,885	2.39	13,059	Outlier
	250	139	2736	385,971	388,707	2736	727,931	730,667	1.44	7897	
	250	139	2736	385,971	388,707	2736	495,245	497,981	1.14	6247	
	250	139	2736	385,971	388,707	2736	500,593	503,329	1.15	6285	
HL1,8–80/20	250	139	4378	154,388	158,766	4378	856,638	861,016	1.91	10,451	Outlier
	250	139	4378	154,388	158,766	4378	174,506	178,884	1.03	5615	
	250	139	4378	154,388	158,766	4378	1,216,746	1,221,124	2.38	13,004	Outlier
	250	139	4378	154,388	158,766	4378	541,254	545,632	1.50	8215	Outlier
	250	139	4378	154,388	158,766	4378	212,600	216,978	1.08	5885	
	250	139	4378	154,388	158,766	4378	162,065	166,443	1.01	5527	
	250	139	4378	154,388	158,766	4378	194,985	199,363	1.05	5760	

Table 14 (continued)

1.8849										
LH1,8–80/20	250	139	4378	154,388	158,766	3462	154,388	157,850	0.83	4557
	250	139	4378	154,388	158,766	6773	154,388	161,161	1.44	7868
	250	139	4378	154,388	158,766	2760	154,388	157,148	0.70	3855
	250	139	4378	154,388	158,766	3951	154,388	158,339	0.92	5046
	250	139	4378	154,388	158,766	2358	154,388	156,746	0.63	3453
	250	139	4378	154,388	158,766	4959	154,388	159,347	1.11	6054
	250	139	4378	154,388	158,766	1775	154,388	156,163	0.52	2870
		No mean stress correction						High residual stresses f(R) = 1.0		
UL1,8–80/20 f(R)1,0	250	139	4378	154,388	158,766	4378	42,840	47,218	0.86	4682
	250	139	4378	154,388	158,766	4378	41,172	45,550	0.85	4670
	250	139	4378	154,388	158,766	4378	30,724	35,102	0.84	4596
	250	139	4378	154,388	158,766	4378	39,842	44,220	0.85	4660
	250	139	4378	154,388	158,766	4378	22,996	27,374	0.83	4541
	250	139	4378	154,388	158,766	4378	34,310	38,688	0.84	4621
	250	139	4378	154,388	158,766	4378	42,283	46,661	0.85	4678
		No mean stress correction						Mean stress correction f(R = 1,8) = 1,3		
UL1,8–80/20 f(R)1,3	250	139	4378	154,388	158,766	4378	42,840	47,218	0.14	4682
	250	139	4378	154,388	158,766	4378	41,172	45,550	0.14	4670
	250	139	4378	154,388	158,766	4378	30,724	35,102	0.13	4596
	250	139	4378	154,388	158,766	4378	39,842	44,220	0.14	4660
	250	139	4378	154,388	158,766	4378	22,996	27,374	0.12	4541
	250	139	4378	154,388	158,766	4378	34,310	38,688	0.13	4621
	250	139	4378	154,388	158,766	4378	42,283	46,661	0.14	4678
PIa 1,8–80/20 8 blocks	250	139	4378	154,388	158,766	4914	152,630	157,544	1.10	5996
	250	139	4378	154,388	158,766	4368	133,551	137,919	0.97	5315
	250	139	4378	154,388	158,766	3276	95,394	98,669	0.72	3952
	250	139	4378	154,388	158,766	3276	95,394	98,669	0.72	3952
	250	139	4378	154,388	158,766	3276	95,394	98,669	0.72	3952
	250	139	4378	154,388	158,766	3276	95,394	98,669	0.72	3952
	250	139	4378	154,388	158,766	3822	114,472	118,294	0.85	4633
PIb1,8–20/80 8 blocks	250	139	1095	617,553	618,648	955	457,889	458,844	0.77	4202
	250	139	1095	617,553	618,648	955	457,889	458,844	0.77	4202
	250	139	1095	617,553	618,648	1365	686,833	688,198	1.14	6234
	250	139	1095	617,553	618,648	1092	534,204	535,296	0.89	4879
	250	139	1095	617,553	618,648	0	0	0	0.00	0
	250	139	1095	617,553	618,648	0	0	0	0.00	0
	250	139	1095	617,553	618,648	0	0	0	0.00	0

Table 15 Test results variable amplitude testing for 1.4678 + CP700

1.4678 + CP700										
Spectrum type	ΔS_h	ΔS_l	$n_{h,spec}$	$n_{l,spec}$	n_{spec}	$n_{h,test}$	$n_{l,test}$	n_{test}	D_V	$N_{äq}$
	[MPa]	[MPa]	[−]	−]	[−]	[−]	[−]	[−]	[−]	[−]
HL1,5–80/20	277	185	1874	14,233	16,106	1,874	12,986	14,860	0.98	2301
	277	185	1874	14,233	16,107	1,874	43,432	45,306	1.41	3303
	277	185	1874	14,233	16,107	1,874	99,808	101,682	2.20	5159
	277	185	1874	14,233	16,107	1,874	18,136	20,010	1.05	2,471
	277	185	1874	14,233	16,107	1,874	49,976	51,850	1.50	3519
	277	185	1874	14,233	16,107	1,874	66,407	68,281	1.73	4059
	277	185	1874	14,233	16,107	1,874	86,813	88,687	2.02	4731
HL1,8–80/20	277	154	1874	66,069	67,942	1,874	49,488	51,362	0.95	2225

Acknowledgements We also thank the University of Kassel, Institute of Material Science, Germany, for performing X-ray diffraction measurements of residual stresses as well as MAN Truck & Bus SE, Munich, Germany and Outokumpu Nirosta GmbH, Krefeld, Germany for manufacturing and sponsoring of the welded specimens.

Funding Open Access funding enabled and organized by Projekt DEAL. The IGF project 19410 N of FOSTA—Forschungsvereinigung Stahlanwendung e. V. Düsseldorf is funded by the Federal Ministry of Economic Affairs and Climate Action (BMWK) via the AiF within the framework of the program for the promotion of the Industrielle Gemeinschaftsforschung (IGF) based on a resolution of the German Bundestag.

Data Availability Data will be made available on request.

Declarations

Conflict of interest The authors declare no competing interests.

References

1. Palmgren A (1924) *Die Lebensdauer von Kugellagern*. Z Ver Dtsch Ing 14:339–341
2. Miner MA (1945) Cumulative damage in fatigue. J Appl Mech 12(3):159–164
3. Kotte KL, Eulitz KG (2007) *Über die Treffsicherheit von Lebensdauervorhersagen und die Nutzung von Datensammlungen.* Kolloquium Betriebsfestigkeits-Berechnung, 30.03.2007, IMA Materialforschung und Anwendungstechnik GmbH
4. Skorupa M (1998) Load interaction effects during fatigue crack growth under variable amplitude loading - a literature review Part I: Empirical trends. Fatigue Fract Eng Mater Struct 21(8):987–1006
5. Skorupa M (1999) Load interaction effects during fatigue crack growth under variable amplitude loading - a literature review Part. II: Qualitative interpretation. Fatigue Fract Eng Mater Struct 22(10):905–926
6. Vormwald M (2015) Classification of load sequence effects in metallic structures. Procedia Eng 101:534–542
7. Eulitz, KG, Döcke H, Esderts A, Kotte KL, Zenner H (1994) *Lebensdauervorhersage I: Vorhaben 152, Verbesserung der Lebensdauerabschätzung durch systematische Aufarbeitung und Auswertung vorliegender Versuchsreihen*, Forschungskuratorium Maschinenbau, Heft 189, Frankfurt
8. Zenner H, Liu J (1992) *Vorschlag zur Verbesserung der Lebensdauerabschätzung nach dem Nennspannungskonzept*. Konstruktion 44(1):9–17
9. Hinkelmann K, Esderts A, Zenner H (2012) *Verbesserung der Lebensdauerabschätzung durch Berücksichtigung des Lebensdauervielfachen*. Materialwissenschaft Werkstofftechnik 43(10):851–863
10. Richart FE, Newmark NM (1948) An hypothesis for the determination of cumulative damage in fatigue. In: Proc. ASTM 48, pp 767–800
11. Marco SM, Starkey WL (2022) A concept of fatigue damage. ASME Trans 76(4):627–632. https://doi.org/10.1115/1.4014922
12. Subramanyan S (1976) A cumulative damage rule based on the knee point of the S-N curve. ASME J Eng Mater Technol 98(4):316–321. https://doi.org/10.1115/1.3443383
13. Manson SS, Halford GR (1986) Re-examination of cumulative fatigue damage analysis – an engineering perspective. Engng Fract Mech 25(5–6):539–571. https://doi.org/10.1016/0013-7944(86)90022-6
14. Manson SS, Halford GR (1981) Practical implementation of the double-linear damage rule and damage curve approach for treating cumulative fatigue damage. Int J Fracture 17:169–192
15. Vormwald M (1989) *Anrißlebensdauervorhersage auf Basis der Schwingbruchmechanik für kurze Risse*. Diss, TU Darmstadt
16. Fatemi A, Yang L (1998) Cumulative fatigue damage and life prediction theories: a survey of the state of the art for homogeneous materials. Int J Fatigue 20(1):9–34
17. Neuhäusler J, Roth J, Oswald M, Dürr A, Rother K (2022) Sequence effects on the life estimation of welded tubular structures made of S355J2H under tension. In 75th IIW Annual Assembly and International Conference. 17th– 22nd July, Tokyo, Japan

18. DIN EN 10219–1:2006-07: Cold formed welded structural hollow sections of non-alloy and fine grain steels – Part 1: Technical delivery conditions. German version EN 10219-1:2006
19. prEN 10088–2:2021: Stainless steels – Part 2: Technical delivery conditions for sheet/plate and strip of corrosion resisting steels for general purposes
20. https://www.outokumpu.com/expertise/2020/build-stronger-and-lighter-vehicle-structures-with-stainless-steel, Accessed 02/14/2022
21. Heidecker C, Lindner S (2020) *Ultrahochfeste Edelstähle*, Verlag Moderne Industrie, München, Die Bibliothek der Technik, Band 404. SZ Scala GmbH; 1. Edition.
22. Deutsches Institut für Normung e.V (2016) *DIN 50100: Schwingfestigkeitsversuch – Durchführung und Auswertung von zyklischen Versuchen mit konstanter Lastamplitude für metallische Werkstoffproben und Bauteile*
23. Krebs J, Hübner P, Kaßner M (2012) *Eigenspannungseinfluss auf Schwingfestigkeit und Bewertung in geschweißten Bauteilen*. DVS-Berichte Bd. 234, 2. Auflage, DVS Media, Düsseldorf
24. Dürr A, Roth J, Rother K, Oswald M, Neuhäusler J: Consideration of sequence effects on the lifetime estimation of hollow section constructions, Final Report, FOSTA P 1195/IGF-Nr. 19410 N (in German)
25. DVS AKuB (2017) Ausschuss für Technik: *Merkblatt DVS 0905 - Industrielle Anwendung des Kerbspannungskonzeptes für den Ermüdungsfestigkeitsnachweis von Schweißverbindungen*. DVS Media GmbH
26. Rother K, Rudolph J (2011) Fatigue assessment of welded structures: practical aspects for stress analysis and fatigue assessment. Fatigue Fract Eng Mater Struct 34(3):177–204
27. Hobbacher AF (2016) Recommendations for fatigue design of welded joints and components, 2nd ed. Springer International Publishing. https://doi.org/10.1007/978-3-319-23757-2
28. Rother K, Fricke W (2016) Effective notch stress approach for welds having low stress concentration. Int J Press Vessels Piping 147:12–20
29. Radaj D, Vormwald M (2013) Advanced methods of fatigue assessment. Springer, Heidelberg
30. ISO 14347:2008-12: Fatigue – Design procedure for welded hollow-section joints – Recommendations. 2008-12.
31. Rother K, Pohl W, Schneider D (2016) Jandkowski U: *Effiziente rechnergestützte Entwicklung von Karosseriekonzepten*. In: ATZ-Fachtagung 14. 10. Karosseriebautage in Hamburg.